EUROFUSION WPJET1-PR(15) 13709

A Bisoffi et al.

Hybrid cancellation of ripple disturbances

Preprint of Paper to be submitted for publication in Automatica

This work has been carried out within the framework of the EUROfusion Consortium and has received funding from the Euratom research and training programme 2014-2018 under grant agreement No 633053. The views and opinions expressed herein do not necessarily reflect those of the European Commission.

This document is intended for publication in the open literature. It is made available on the clear understanding that it may not be further circulated and extracts or references may not be published prior to publication of the original when applicable, or without the consent of the Publications Officer, EUROfusion Programme Management Unit, Culham Science Centre, Abingdon, Oxon, OX14 3DB, UK or e-mail Publications.Officer@euro-fusion.org

Enquiries about Copyright and reproduction should be addressed to the Publications Officer, EUROfusion Programme Management Unit, Culham Science Centre, Abingdon, Oxon, OX14 3DB, UK or e-mail Publications.Officer@euro-fusion.org

The contents of this preprint and all other EUROfusion Preprints, Reports and Conference Papers are available to view online free at http://www.euro-fusionscipub.org. This site has full search facilities and e-mail alert options. In the JET specific papers the diagrams contained within the PDFs on this site are hyperlinked

Hybrid cancellation of ripple disturbances

Andrea Bisoffi [c,1] Mauro Da Lio [c,1] Luca Zaccarian [b,c,2] Daniele Carnevale [d,3] and JET Contributors [a]

EUROfusion Consortium, JET, Culham Science Centre, Abingdon, OX14 3DB, UK

[a] *See the Appendix of F. Romanelli et al., Proceedings of the 25th IAEA Fusion Energy Conference 2014, Saint Petersburg, Russia.*

[b] *CNRS, LAAS, 7 avenue du colonel Roche, F-31400 Toulouse, France and Univ. de Toulouse, LAAS, F-31400 Toulouse, France.*

[c] *Dipartimento di Ingegneria Industriale, University of Trento, Italy*

[d] *Dipartimento di Ing. Civile e Ing. Informatica, University of Rome "Tor Vergata", Italy*

Abstract

In this paper we propose a novel model of the ripple produced in different contexts involving switching power electronics. The novelty of this model is that the nonsmooth waveform characterizing the ripple is captured by a suitable hybrid dynamics performing state jumps at the switching instants. In addition to showing that this model is effective at representing the ripple waveform, we propose two hybrid schemes ensuring asymptotic observation of the ripple waveform, one of them using knowledge of the switching instants and a second one without knowledge of the switching instants. Simulation results illustrate the effectiveness of the proposed hybrid observation laws.

Key words: hybrid dynamical system, hybrid observer, power system, Tokamak plasma, ripple

1 Introduction

Many engineering applications require power electronics in their actuators and often these power electronics are equipped with converters from AC to DC power supply. These converters typically arise from switching electronics that automatically select the maximum voltage difference among the available alternating waveforms, so to obtain an almost direct current at the output (see, e.g., the description in Section 2). Similarly, DC motors are often equipped with split ring commutators on their shaft, so that the maximum available torque is generated by the rotor coils that are instantaneously (almost) orthogonal to the stator magnetic field. In both these cases, the desired constant output is affected by a peculiar periodic nonsmooth disturbance, typically called "ripple", whose nonsmooth points correspond to the instants of commutation of the electronic components.

Ripple disturbances may have damaging effects on control design, not only because they affect the actuation signal (like in a DC motor), but also because they often affect the power supply, thus possibly affecting all sensor measurements due to the magnetic coupling. This phenomenon is especially seen in high-power applications such as Tokamak plasmas control [1]. One of the important features of this disturbance is that the frequency of the ripple is typically a known parameter with little uncertainty, because it is a multiple of the utility frequency in the electrical power grid, which is in turn tuned very finely to the values of either 50 or 60 Hz. Due to this fact, it appears natural to address the problem of ripple esti-

[1] Email: {andrea.bisoffi, mauro.dalio}@unitn.it.

[2] Work supported by the ANR project LimICoS contract number 12 BS03 005 01, and by HYCON2 Network of Excellence "Highly-Complex and Networked Control Systems", grant agreement 257462. Email: zaccarian@laas.fr.

[3] Work supported by ENEA-EUROFUSION. This work has been carried out within the framework of the EUROfusion Consortium and has received funding from the Euratom research and training programme 2014-2018 under grant agreement No 633053. The views and opinions expressed herein do not necessarily reflect those of the European Commission. E-mail: daniele.carnevale@uniroma2.it

mation and rejection using linear [2] or nonlinear [3, Ch. 8] regulation theory.

The peculiar non-smoothness of ripple disturbances however makes it less prone to be addressed with classical continuous-time approaches and makes it an interesting problem to be tackled using hybrid regulation theory (see, e.g., the preliminary work in [4] and the more recent results in [5–8] and references therein). Those works, as well as the approach that we adopt here, are based on the novel framework for the description of nonlinear hybrid dynamical systems in [9, 10]. The peculiarity of hybrid regulation theory is that, as extensively discussed in the above cited works, the state of the exosystem experiences jumps, therefore the hybrid internal model implemented in the regulator (or in the observer, as in our case) must jump at suitable times. Two main approaches naturally arise: that one of the situation where the jump times (or the clock as mentioned in [11]) is available for measurement – which in our case would correspond to having access to the switching instants of the power electronics – and that one where the jump times are not available. Based on these two main situations we give here two solutions to the estimation of the ripple signal, by introducing suitable hybrid observation laws. Our approach is much inspired by the recent results in [12] and the machinery given in [13, Thm 2] (also reported in [14, Lemma 1] with a notation that resembles more closely the situation addressed here). We would also like to emphasize that a hybrid approach to tackle this problem is not compulsory, because the ripple disturbance is indeed an absolutely continuous function and one may find ways to generate with a nonsmooth continuous time approach (see, e.g., the results in [15] where a continuous-time exosystem is built that generates the absolute value of a cosine waveform). Our results are also close in nature to those reported in [5, §4.2], where a hybrid exosystem generates the absolute value of a cosine waveform. However, as compared to that result, we focus here on ripple signals that perform commutations at phases *different* from $\pm\pi/2$. A preliminary version of this paper was presented in [16]. Here, as compared to [16], we give the proofs of our two main theorems, and we discuss the application of the proposed scheme to the experimental signals of the JET Tokamak, whereas only simulation results were given in [16].

The paper is organized as follows: in Section 2 we introduce the hybrid model for the ripple generation and present the estimation problem under consideration. In Sections 3 and 4 we illustrate the two proposed estimation schemes and state and prove their desirable properties. Finally, in Section 5 we illustrate the effectiveness of our schemes by simulations.

2 A hybrid model for the ripple-induced noise in measurement signals

In this section we will deal with the modelling of the ripple through a hybrid system.

Let us consider a simple physical example where the ripple arises, i.e. the three phase diode bridge rectifier depicted in Figure 1. This device converts a three-phase voltage to a mono-phase *almost* direct voltage, which can be then applied, for example, to a load resistor. The resulting voltage is *almost* direct because the logic of conversion, which we are going to explain, is such that a non smooth waveform, the ripple, is superposed to the ideal direct voltage.

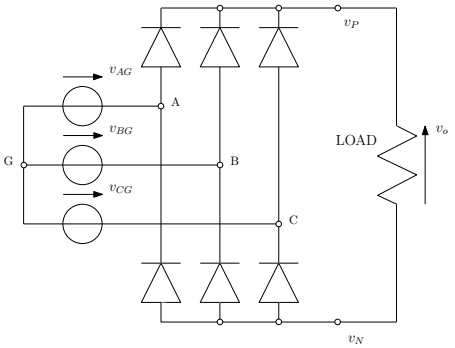

Figure 1. A three phase diode bridge rectifier for conversion from AC to DC, which results in a waveform affected by a ripple.

The valves in Figure 1 are ideal diodes, and the three phase voltages have the form:

$$\begin{aligned} v_{AG} &= v_A - v_G = V_f \sin\Big(\omega t + \theta_0\Big) \\ v_{BG} &= v_B - v_G = V_f \sin\Big(\omega t + \theta_0 - \frac{2\pi}{3}\Big) \\ v_{CG} &= v_C - v_G = V_f \sin\Big(\omega t + \theta_0 - \frac{4\pi}{3}\Big), \end{aligned} \tag{1}$$

where G stands for *ground*. The following lemma is easily derived.

Lemma 1 *Given the supply in (1), the output voltage of the converter in Figure 1 is*

$$v_o = \sqrt{3} V_f \max_{i\in\mathbb{Z}} \cos\Big(\omega t + \theta_0 - i\frac{\pi}{3}\Big). \tag{2}$$

Proof. Without loss of generality, we can set $\theta_0 = 0$ in (1). Then, $v_o = v_P - v_N = v_{PG} - v_{NG}$ can be determined using the known rules in electronics that establish which diode is conducting among more than one connected at cathode or anode. We get then from standard results in circuit theory:

$$
\begin{aligned}
&v_o = v_{PG} - v_{NG} = \\
&= \max_{i\in\mathbb{Z}} \left\{ V_f \sin\left(\omega t - i\frac{2\pi}{3}\right) \right\} - \min_{j\in\mathbb{Z}} \left\{ V_f \sin\left(\omega t - j\frac{2\pi}{3}\right) \right\} \\
&= \max_{i,j\in\mathbb{Z}} \left\{ V_f \sin\left(\omega t - i\frac{2\pi}{3}\right) - V_f \sin\left(\omega t - j\frac{2\pi}{3}\right) \right\} \\
&= V_f \max_{i,j\in\mathbb{Z}} \left\{ 2\cos\left(\omega t - (i+j)\frac{\pi}{3}\right) \sin\left((j-i)\frac{\pi}{3}\right) \right\} \\
&= \sqrt{3} V_f \max_{i\in\mathbb{Z}} \Bigg\{ \underbrace{\cos\left(\omega t - (2i+1)\frac{\pi}{3}\right)}_{j-i=1}, \underbrace{\cos\left(\omega t - (2i+2)\frac{\pi}{3}\right)}_{j-i=2}, \\
&\qquad \underbrace{-\cos\left(\omega t - (2i-1)\frac{\pi}{3}\right)}_{j-i=-1}, \underbrace{-\cos\left(\omega t - (2i-2)\frac{\pi}{3}\right)}_{j-i=-2} \Bigg\} \\
&= \sqrt{3} V_f \max_{i\in\mathbb{Z}} \cos\left(\omega t - i\frac{\pi}{3}\right),
\end{aligned}
$$

where the last step can be carried out via graphical inspection. □

Remark 1 In Figure 2 we depicted the three line-to-line voltages and their opposites in sign. The maximum among the six voltages is then exactly the expression v_o in (2) and is represented in Figure 2 by a bold dashed line. ⌟

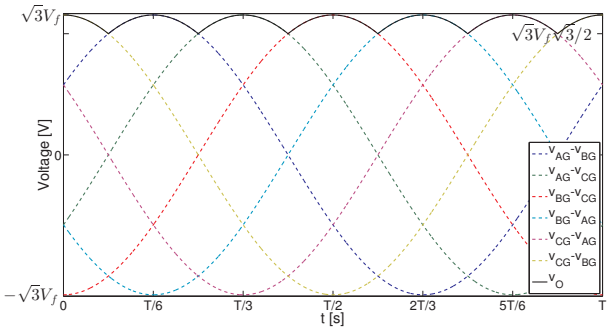

Figure 2. Line-to-line voltages in a three-phase diode bridge rectifier.

We propose below a different characterization of the ripple, based on a hybrid model. We will notice in Proposition 1 how this formulation can represent the physical example that we have just introduced. Consider the following hybrid model:

$$
\begin{cases} \dot{x}_r = \begin{bmatrix} 0 & -\omega \\ \omega & 0 \end{bmatrix} \begin{bmatrix} x_{r1} \\ x_{r2} \end{bmatrix} = A_r x_r & (x_r, \bar{b}) \in \mathcal{C} \\ \dot{\bar{b}} = 0, \end{cases} \tag{3a}
$$

$$
\begin{cases} x_r^+ = \begin{bmatrix} 1 & 0 \\ 0 & -1 \end{bmatrix} \begin{bmatrix} x_{r1} \\ x_{r2} \end{bmatrix} = J_r x_r & (x_r, \bar{b}) \in \mathcal{D}, \\ \bar{b}^+ = \bar{b}, \end{cases} \tag{3b}
$$

where sets $\mathcal{C}$ and $\mathcal{D}$ are specified below, and we use the following output equations:

$$
y_r = x_{r1} + \bar{b} = \begin{bmatrix} 1 & 0 \end{bmatrix} x_r + \bar{b} = C_r x_r + \bar{b} \tag{4a}
$$

$$
\theta = \angle(x_r). \tag{4b}
$$

Output y_r in (4a) is the measured signal and θ is *not* available for measurement (even though we may assume knowledge of its transition times). Function $\angle(\cdot)$ returns the phase of the vector at the argument, namely for each $x_r \neq 0$ it is the only angle $\theta \in [-\pi, \pi)$ satisfying $x_r = |x_r| \begin{bmatrix} \cos(\theta) \\ \sin(\theta) \end{bmatrix}$, which is well defined for all x_r satisfying $|x_r| \neq 0$. Note that function $\angle(\cdot)$ resembles the well known function atan2$(\cdot,\cdot)$ used in the robotics context.

The jump and flow sets in (3) are defined as:

$$
\mathcal{K} = \{(x_r, \bar{b}) \colon \delta \leq |x_r| \leq \Delta, |\bar{b}| \leq \Delta \text{ with } \Delta \geq \delta > 0\} \tag{5a}
$$

$$
\mathcal{C} = \{(x_r, \bar{b}) \colon -\pi/6 \leq \theta \leq \pi/6\} \cap \mathcal{K} \tag{5b}
$$

$$
\mathcal{D} = \{(x_r, \bar{b}) \colon \theta = \pi/6\} \cap \mathcal{K} \tag{5c}
$$

and are depicted in Figure 3, where we added a possible solution to (3) flowing in $\mathcal{C}$ and jumping when it reaches $\mathcal{D}$. In $\mathcal{C}$ and $\mathcal{D}$, we impose the intersection with set $\mathcal{K}$ in order to exclude two extreme situations. (i) We choose δ strictly positive, which may be arbitrarily small, because we need to ensure that the function in (4b) be well defined; the case $\delta = 0$ corresponds to no ripple at all. (ii) We choose Δ as a finite upper bound, which may be arbitrarily large, because we assume the ripple to be bounded. This allows us to deal with compact sets in our design and to rely on useful results from [9, Ch. 7]. Nowhere in our design the knowledge of the values of δ and Δ is required.

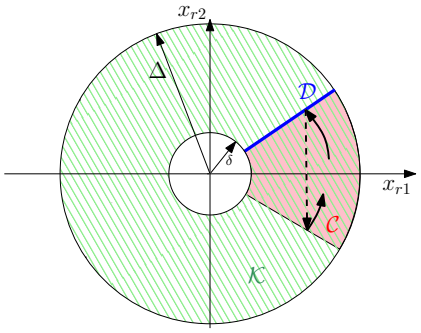

Figure 3. Flow set, jump set and quantities δ, Δ of set $\mathcal{K}$. A possible trajectory is depicted, with solid arrow for the flow and dashed arrow for a jump.

Remark 2 If the ripple was not generated by a three phase system, we would consider a different angle in (5b) and (5c) instead of $\pi/6$. For example, for a 6-phase or a 12-phase system the angle would be respectively $\pi/12$ or $\pi/24$. ⌟

The following straightforward result motivates the study carried out in this paper and hybrid model (3). Notice that we constrain θ_0 to be in the set $[-\pi/6, \pi/6]$ because any other value of θ_0 could be shifted to this interval without changing the resulting value of v_o in (2).

Proposition 1 *For any value of $\theta_0 \in [-\pi/6, \pi/6]$ and $V_f > 0$ in (2), there exist initial conditions $x_r(0,0) = \sqrt{3}V_f \left[\begin{smallmatrix}\cos\theta_0\\ \sin\theta_0\end{smallmatrix}\right]$ and $\bar{b}(0,0) = 0$ such that the unique solution to (3)–(5) has unbounded domain in the ordinary time direction and satisfies $y_r(t,j) = v_o(t)$, for all $(t,j) \in dom(y_r)$.*

Proof. We carry out the proof in polar coordinates that are globally defined in $\mathcal{C} \cup \mathcal{D}$. First note that from standard polar coordinates representation of linear oscillators, output θ in (4b) evolves along flows according to relation $\dot{\theta} = \omega$. Moreover, notice that the definition of jump set in (5) and the jump law in (3b) ensures that as soon as $\theta = \pi/6$, one has (in polar coordinates):

$$\left(|x_r| \begin{bmatrix}\cos(\pi/6)\\ \sin(\pi/6)\end{bmatrix}\right)^+ = J_r|x_r| \begin{bmatrix}\cos(\pi/6)\\ \sin(\pi/6)\end{bmatrix} = |x_r| \begin{bmatrix}\cos(-\pi/6)\\ \sin(-\pi/6)\end{bmatrix},$$

showing that $|x_r|$ remains constant and θ changes sign across jumps. Therefore, each pair of consecutive jumps witnesses a dwell time of exactly $\pi/(3\omega)$ which is the time for θ to flow again from $-\pi/6$ to $\pi/6$. This shows dwell time of all solutions and proves that the domain of all solutions is unbounded in the ordinary time direction. Uniqueness of solution follows from the fact that along flows and across jumps, the flow and jump maps are Lipschitz single valued functions, in addition to the fact that no flow is possible from the jump set because the flow map $\dot{\theta} = \omega$ points out of $\mathcal{C} \cup \mathcal{D}$ (more formally, its intersection with the tangent cone to $\mathcal{C} \cup \mathcal{D}$ is empty – see [9, Prop. 6.10]).

Moreover, one easily gets that $\frac{d}{dt}|x_r| = 0$ along flows. Combining this relation with the fact that θ keeps revolving in the set $[-\pi/6, \pi/6]$, where $\cos(\theta)$ assumes its maximum, we get that all solutions starting from $\bar{b}(0,0) = 0$ satisfy:

$$\begin{aligned} y_r(t,j) &= x_{r1}(t,j) = |x_r(t,j)|\cos(\theta(t,j)) \\ &= |x_r(0,0)| \max_{i\in\mathbb{Z}} \cos\left(\theta(0,0) + \omega t - i\frac{\pi}{3}\right). \end{aligned} \tag{6}$$

Then it is readily seen from (6) that choosing the initial conditions $x_r(0,0) = \sqrt{3}V_f \left[\begin{smallmatrix}\cos\theta_0\\ \sin\theta_0\end{smallmatrix}\right]$ and $\bar{b}(0,0) = 0$, the (unique) solution to (3)–(5) satisfies the claim. □

In light of Proposition 1, the goal of this paper can be formulated as that of asymptotic rejection of the zero-mean disturbance

$$\begin{aligned} d(t) &= v_o(t) - \frac{\omega}{2\pi}\int_0^{\frac{2\pi}{\omega}} v_o(\tau)d\tau = v_o(t) - \frac{3\sqrt{3}V_f}{\pi} \\ &= y_r(t,j) - \bar{b}(t,j) - \frac{3}{\pi}|x_r(t,j)| \end{aligned}$$

so that

$$d(t) = x_{r1}(t,j) - \frac{3}{\pi}|x_r(t,j)|, \tag{7}$$

where for the integral we used that $\frac{\omega}{2\pi}\int_0^{\frac{2\pi}{\omega}} v_o(\tau)d\tau = \frac{6\omega}{2\pi}\int_{-\frac{2\pi}{12\omega}-\frac{\theta_0}{\omega}}^{\frac{2\pi}{12\omega}-\frac{\theta_0}{\omega}} \sqrt{3}V_f\cos(\omega\tau+\theta_0)d\tau = \frac{3\sqrt{3}V_f}{\pi}$. The introduction of a constant bias $\bar{b}$ in in (3) and (4) serves the purpose of modeling the situation where the measurement $y_r(t)$ of a desirable signal $\sigma(t)$ is affected by a disturbance $d(t)$, $t \geq 0$. Then equation (7) shows that in our hybrid ripple model, σ is represented by the constant DC component $\bar{b} + \frac{3}{\pi}|x_r|$ while the disturbance d is the zero mean signal $x_{r1} - \frac{3}{\pi}|x_r|$. In particular, we may assume signal σ to be slowly varying as compared to the time-scale of d in (7), so that it can be considered as constant in our analysis, based on the observations of [10, Corollary 7.27]. We are using precisely this robustness result in Section 5 when we are considering JET experimental measurements where a ripple-shaped disturbance is superimposed to a low frequency signal.

In the next two sections we propose two hybrid schemes to estimate the disturbance d in (7) from the measurement of y_r. The first scheme addresses the simplified setting where the switching instants of the hybrid model are known and the second one relies on an estimator of the output θ to remove this assumption.

3 Ripple estimation with knowledge of switching instants

If the switching instants of the ripple generator in (3)–(5) are known, it is possible to design an estimator consisting in a suitable Luenberger observer during flows and that performs simultaneous jumps with the ripple generator (namely, the jump and flow sets remain unchanged and do *not* depend on the observer states). This corresponds to a simplified setting for the observer design. The architecture of the proposed solution is sketched in Figure 4.

The assumption that the switching instants of the hybrid ripple generator are available to the ripple observer may be verified, for example, if the observation algorithm is somehow connected to the circuitry commanding the switches of the rectifier in Figure 1, so that the switching times are known. Another case is that of a torque ripple generated by a DC motor where one may assume to

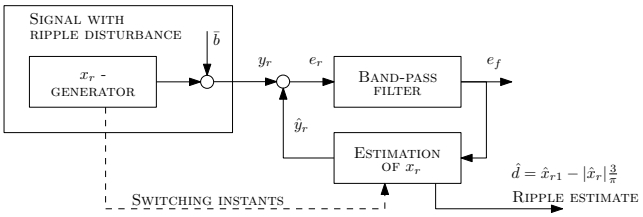

Figure 4. Scheme with generator, filter and hybrid observer of x_r when the switching instants are known.

measure the shaft angle and then compute the switching times based on the position of the split ring commutator.

Let us introduce the elements of Figure 4. The block "Signal with ripple disturbance" corresponds to hybrid system (3)–(5). To eliminate the effect of the bias from y_r, we introduce the band-pass filter:

$$F(s) = \frac{\frac{s}{\omega}}{\left(1+\frac{s}{\omega}\right)^2}, \tag{8}$$

with a double pole at the ripple frequency $\omega/(2\pi)$ that helps isolating the dominant modes of the (nonsmooth) signal to be estimated from the constant bias and the high-frequency noise.

For the following derivations we use a state-space form for filter (8), with matrices:

$$\left[\begin{array}{c|c} A_f & B_f \\ \hline C_f & \end{array}\right] = \left[\begin{array}{cc|c} 0 & 1 & 0 \\ -\omega^2 & -2\omega & 1 \\ \hline 0 & \omega & \end{array}\right]. \tag{9}$$

Then we augment equations (3) with the following flow and jump equations comprising the observer and filter dynamics.

$$\begin{cases} \dot{x}_f = A_f x_f + B_f(y_r - \hat{y}_r) \\ \dot{\hat{x}}_r = A_r \hat{x}_r + L e_f, \end{cases} \quad (x_r, \bar{b}) \in \mathcal{C} \tag{10a}$$

$$\begin{cases} x_f^+ = x_f \\ \hat{x}_r^+ = J_r \hat{x}_r, \end{cases} \quad (x_r, \bar{b}) \in \mathcal{D}, \tag{10b}$$

where the Luenberger gain is $L = \left[\begin{smallmatrix} \ell \\ 0 \end{smallmatrix}\right]$ and scalar ℓ is a positive design parameter. We augment equation (4a) with the other output equations:

$$\begin{aligned} e_f &= C_f x_f \\ \hat{y}_r &= C_r \hat{x}_r \\ \hat{d} &= \hat{x}_{r1} - |\hat{x}_r|\frac{3}{\pi}, \end{aligned} \tag{11}$$

where $\hat{d}$ is the zero-mean estimate of the ripple signal (7). Notice that the flow and jump sets are unchanged and only depend on output θ in (4b). We emphasize that to implement hybrid observer (10) no measurement of θ is necessary, but it is necessary to know the switching times, that is the times when the observer state $\hat{x}_r$ should jump.

To suitably analyze the overall system (3)-(5), (9), (10), (11), let us introduce the error variable

$$e := \begin{bmatrix} \tilde{x}_r \\ \tilde{x}_f \end{bmatrix} := \begin{bmatrix} x_r - \hat{x}_r \\ x_f + A_f^{-1} B_f \bar{b} \end{bmatrix}, \tag{12}$$

where $\tilde{x}_r$ is the error related to the ripple generation and $\tilde{x}_f$ is a coordinate transformation of the state variables of the filter chosen to satisfy $A_f \tilde{x}_f = A_f x_f + B_f \bar{b}$. The output equation

$$d - \hat{d} = \begin{bmatrix} 1 & 0 & 0 & 0 \end{bmatrix} e + \frac{3}{\pi}(|\hat{x}_r| - |x_r|), \tag{13}$$

corresponding to the disturbance estimation error, readily follows from expressions (7), (11) and (12).

It can be readily checked that the (hybrid) error dynamics corresponds to

$$\dot{e} = \begin{bmatrix} A_r & -LC_f \\ B_f C_r & A_f \end{bmatrix} e = A_e e, \quad (x_r, \bar{b}) \in \mathcal{C} \tag{14a}$$

$$e^+ = \begin{bmatrix} J_r & 0 \\ 0 & I_2 \end{bmatrix} e = J_e e, \quad (x_r, \bar{b}) \in \mathcal{D} \tag{14b}$$

thanks to the fact that $\dot{\bar{b}} = 0$ and $C_f A_f^{-1} B_f = 0$. Then we can state the next result.

Lemma 2 *Given dynamics (3)-(5), (9), (10), (11), and the error dynamics (14), for any $\ell > 0$, the selection $L = \left[\begin{smallmatrix} \ell \\ 0 \end{smallmatrix}\right]$ in (10a) and (14a) is such that there exist $P = P^T > 0$ and $H \in \mathbb{R}^{1\times 4}$ such that (H, A_e) is an observable pair and function*

$$V(e) = e^T P e \tag{15}$$

satisfies

$$\langle \nabla V(e), A_e e \rangle \leq -e^T H^T H e, \quad (x_r, \bar{b}) \in \mathcal{C} \tag{16a}$$

$$V(J_e e) - V(e) = 0, \quad (x_r, \bar{b}) \in \mathcal{D}. \tag{16b}$$

Proof. Consider the diagonal selection $P = \left[\begin{smallmatrix} 1 & 0 & 0 & 0 \\ 0 & 1 & 0 & 0 \\ 0 & 0 & \omega^3\ell & 0 \\ 0 & 0 & 0 & \omega\ell \end{smallmatrix}\right]$. From condition $\ell > 0$ it clearly follows $P = P^T > 0$. Moreover, using A_e in (14a), one obtains $\mathrm{He}(PA_e) =$

$\begin{bmatrix} 0&0&0&0\\ 0&0&0&0\\ 0&0&0&0\\ 0&0&0&-4\omega^2\ell \end{bmatrix} = -H^TH$, and $H = \begin{bmatrix} 0&0&0&2\omega\sqrt{\ell} \end{bmatrix}$. Then (16a) readily follows. Regarding matrix H, observability of pair (A_e, H) can be easily checked by computing the observability matrix $\mathcal{O} = \begin{bmatrix} H^T & (HA_e)^T & (HA_e^2)^T & (HA_e^3)^T \end{bmatrix}^T$, whose determinant is $-16\omega^9\ell^2$. Finally, equation (16b) can be checked as follows:

$$\begin{aligned} V^+ - V &= V(e^+) - V(e) = V(J_e e) - V(e) \\ &= e^T J_e^T P J_e e - e^T P e \\ &= e^T \left[\begin{array}{c|cc} J_r^T J_r & 0 & \\ \hline & p_3 & 0 \\ 0 & 0 & p_4 \end{array}\right] e - e^T P e = 0 \end{aligned}$$

because $J_r^T J_r = I_2$. □

Remark 3 Notice that the proof of Lemma 2 applies for any selection of the jump instants. Therefore the scheme in Figure 4 is effective at estimating ripple y_r also when the jump set $\mathcal{D}$ is empty, which boils down to a standard linear disturbance rejection problem with an internal model. Due to this fact, our scheme can be seen as a generalization of the last one, much related to the recent works in [5–8] and references therein. ⌟

Based on the Lyapunov construction of Lemma 2 we can now state our first main result establishing asymptotic estimation of the ripple signal.

Theorem 1 *For any $\ell > 0$, the selection $L = \begin{bmatrix} \ell \\ 0 \end{bmatrix}$ in (10a) and in (14a) guarantees that the compact attractor*

$$\mathcal{A} = \{(x_r, \bar{b}, \hat{x}_r, x_f) : \ e = 0 \text{ and } (x_r, \bar{b}) \in \mathcal{K}\},$$

is uniformly globally exponentially stable for the closed-loop dynamics (3)-(5), (9), (10), (11).

Proof. The result is a direct consequence of [13, Thm 2] (see also [14, Lemma 1] where a parallel formulation to this one is used) with the Lyapunov function of Lemma 2. □

Remark 4 Note that in light of the output equation (13), Theorem 1 implies that for any positive choice of the scalar parameter ℓ, the estimate $\hat{d}$ uniformly and exponentially converges to the ripple disturbance d. Smaller selections of ℓ lead to slower convergence but are less sensitive to noise, whereas larger selections of ℓ lead to faster convergence but larger noise sensitivity should be expected. ⌟

4 Ripple estimation without knowledge of switching instants

In most practical cases it is not easy if not impossible to know the switching instants and the scheme of the previous section cannot be implemented. To address this situation, we present here an enhanced estimation scheme, whose structure is represented in Figure 5. In this new scheme, we estimate the switching instants by building an estimate $\hat{\theta}$ of the unavailable output θ in (4b).

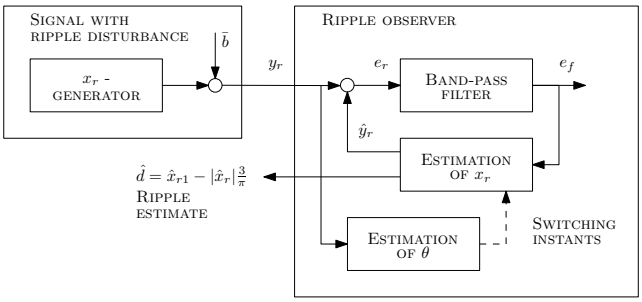

Figure 5. Scheme with generator, estimation of the switching instants, filter and hybrid observer of x_r when the switching instants are *not* known.

Remark 5 In the sequel, to keep the notation simple, we will introduce several coupled dynamical systems comprising different components of the proposed scheme and having different jump and flow sets. These jump and flow sets will be specified in terms of only some state variables, implicitly meaning that the other state variables may assume any value in the specified set. With this simplified notation we refer to the hybrid system constructed having flow set corresponding to the intersection of all the specified flow sets, flow map arising from stacking up all the specified flow equations (no flow equations will be repeated thus generating no ambiguity), jump set corresponding to the union of all the jump sets and jump map corresponding to the union of all the specified jump maps. ⌟

Using the simplified notation mentioned in Remark 5, we preserve the main dynamics in (10) by using a jump rule triggered by the new state $\hat{\theta}$:

$$\begin{cases} \dot{x}_f = A_f x_f + B_f(y_r - \hat{y}_r) \\ \dot{\hat{x}}_r = A_r \hat{x}_r + L e_f \\ \dot{\hat{\theta}} = \omega, \end{cases} \qquad \hat{\theta} \in \left[-\frac{\pi}{3}, \frac{\pi}{6}\right] \tag{17a}$$

$$\begin{cases} x_f^+ = x_f \\ \hat{x}_r^+ = J_r \hat{x}_r \\ \hat{\theta}^+ = \hat{\theta} - \pi/3, \end{cases} \qquad \hat{\theta} \in \left[\frac{\pi}{6}, \frac{\pi}{3}\right] \tag{17b}$$

and preserve the same output equations (11). Note that the lower bound on $\hat{\theta}$ in (17a) and the upper bound in (17b) are coarser than those in (5), because we want to leave some margin for suitable adaptation of $\hat{\theta}$.

Clearly, dynamics (17) converges to the right estimate when $\hat{\theta} = \theta$. The scheme is then completed by inserting an additional logic performing periodic updates on $\hat{\theta}$ in such a way that it converges to θ. Such convergence will be established based on the Lyapunov function:

$$i^* := \underset{i\in\mathbb{Z}}{\operatorname{argmin}} \left(\theta - \hat{\theta} + i\frac{\pi}{3}\right)^2, \tag{18}$$

$$\tilde{\theta} := \theta - \hat{\theta} + i^*\frac{\pi}{3}, \tag{19}$$

$$V_\theta(\theta, \hat{\theta}) := \min_{i\in\mathbb{Z}} \left(\theta - \hat{\theta} + i\frac{\pi}{3}\right)^2 = \tilde{\theta}^2. \tag{20}$$

In particular, the following lemma will be fundamental to achieve this convergence property.

Lemma 3 *Consider any hybrid solution to (3)–(5), (17). The output $\tilde{\theta}$ defined in (19) and the Lyapunov function V_θ in (20) both remain constant along flows and across jumps.*

Moreover, defining[4] *for each $t \geq 0$ the function $j^*(t) = \max_{(t,j)\in\mathrm{dom}\theta} j$, the next identity holds:*

$$\int_t^{t+\frac{\pi}{3\omega}} \hat{\theta}(\tau, j^*(\tau))d(\tau, j^*(\tau))d\tau = -|x_r(0,0)|\rho(\tilde{\theta}), \tag{21}$$

where ρ is such that $\rho(\tilde{\theta})\tilde{\theta}$ is a positive definite function in the interval $\tilde{\theta} \in (-\pi/6, \pi/6)$ and d is the output at the third line of (7), corresponding to $d = |x_r|\cos(\theta) - \frac{3}{\pi}|x_r|$.

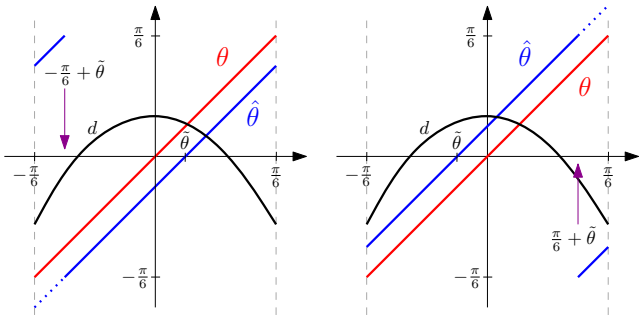

Figure 6. Graphical proof for $\tilde{\theta} > 0$ (left) and $\tilde{\theta} < 0$ (right).

Proof. The fact that $\tilde{\theta}$ and V_θ remain constant along solutions is readily verified by checking that $\dot{\theta} - \dot{\hat{\theta}} = \omega - \omega = 0$ along flows and that $\theta^+ = \theta - \frac{\pi}{3}$ (and similarly for $\hat{\theta}^+$) so that quantity i^* in (18) changes but the minimum in (20) does not change across jumps.

[4] Note that the definition of $j^*(t)$ is valid for all $t \geq 0$ because all solutions have unbounded domain in the ordinary time direction, as established in Proposition 1.

Regarding integral (21), we compute it by dividing the analysis in the two cases shown in Figure 6. After some calculations, essentially splitting each integral in two parts, it is shown that

$$\rho(\tilde{\theta}) = \begin{cases} -\frac{1}{6\omega}\left(\pi - 6\tilde{\theta} - 2\pi\sin\left(\frac{\pi}{6} - \tilde{\theta}\right)\right) = \rho_p(\tilde{\theta}) & \tilde{\theta} \geq 0 \\ -\rho_p(-\tilde{\theta}) & \tilde{\theta} < 0 \end{cases}$$

so that $\rho(\tilde{\theta})\tilde{\theta}$ is positive definite in $(-\pi/6, \pi/6)$, as to be proven. □

Remark 6 Note that, as graphically illustrated in Figure 6, scalar $\tilde{\theta}$ characterized in Lemma 3 is the difference between θ and $\hat{\theta}$ modulo $\pi/3$, that is, recognizing that both θ and $\hat{\theta}$ revolve in the set $[-\pi/6, \pi/6]$ one measures their distance ignoring the jumps so that this distance remains constant despite the jumps of the two variables. ⌟

Based on the preliminary result of Lemma 3, we can now complete the hybrid observer with an additional dynamics implementing integral (21) and imposing suitable jump rules on $\hat{\theta}$ to ensure its convergence to θ. Let us consider

$$\begin{cases} \dot{\bar{y}}_r = 0 \\ \dot{\bar{y}}_{rI} = y_r - \bar{y}_r \\ \dot{\eta} = \hat{\theta}(y_r - \bar{y}_r) \\ \dot{\tau} = 1, \end{cases} \qquad \tau \leq \frac{\pi}{3\omega} \tag{22a}$$

$$\begin{cases} \bar{y}_r^+ = \bar{y}_r + k_{av}\dfrac{3\omega}{\pi}y_{rI} \\ \bar{y}_{rI}^+ = 0 \\ \eta^+ = 0 \\ \tau^+ = 0 \\ \hat{\theta}^+ = \hat{\theta} - \mathrm{sat}_{\frac{\pi}{6}}(k_\theta\eta), \end{cases} \qquad \tau = \frac{\pi}{3\omega}, \tag{22b}$$

where $k_{av} \in (0, 1]$ and $k_\theta > 0$ are two positive gains to be tuned, and function $\mathrm{sat}_{\frac{\pi}{6}}$ is the scalar symmetric saturation function whose output is limited within $[-\pi/6, \pi/6]$. Note that this limitation ensures that $\hat{\theta}^+$ will always belong to the set $[-\pi/3, \pi/3]$, where dynamics (17) ensures existence of solutions.

In (22), state τ is a periodic timer ensuring that integral (21) is computed periodically; state $\bar{y}_{rI}$ integrates output y_r to estimate its average value, whose estimate is stored in $\bar{y}_r$ (updated at each jump based on the latest estimate) and finally η implements integral (21) by subtracting the (estimated) average value $\bar{y}_r$ from measurement y_r and multiplying it by $\hat{\theta}$.

The overall ripple estimation scheme corresponds to plant (3)–(5), the estimator dynamics in (17), and the

extra states and jump rules in (22), where the role of the different jump and flow sets should be intended as explained in Remark 5. The overall state is then given by

$$\xi = (x_r, \bar{b}, x_f, \hat{x}_r, \hat{\theta}, \bar{y}_r, \bar{y}_{rI}, \eta, \tau),$$

where it is emphasized that due to the fact that $(x_r, \bar{b})$ belongs to the compact set $\mathcal{K}$ and $\tau \in [0, \pi/(3\omega)]$, then there exists a large enough scalar M such that $(\bar{y}_r, \bar{y}_{rI}, \eta, \tau) \in M\mathbb{B}^4$, where $\mathbb{B}^4$ is the four-dimensional closed unit ball. In the next theorem we establish parallel results to those of Theorem 1 in terms of stability properties of the attractor

$$\mathcal{A}_e = \mathcal{A} \times [-\pi/3, \pi/3] \times M\mathbb{B}^4, \tag{23}$$

where $\mathcal{A}$ is defined in (1) and corresponds to the set where the estimate is correct. Note that Theorem 2 only establishes local properties of the scheme even though its results could be strengthened by relying on a more sophisticated update law for $\hat{\theta}$ (see, e.g., [17] for global asymptotic stabilization of dynamics on bounded manifolds like our angles θ and $\hat{\theta}$) and on global results on cascaded hybrid systems.

Theorem 2 *For any $\ell > 0$, any $k_{av} \in (0, 1]$ and a small enough value of $k_\theta > 0$, the selection $L = \left[\begin{smallmatrix} \ell \\ 0 \end{smallmatrix}\right]$ in (17) guarantees that the compact attractor $\mathcal{A}_e$ is uniformly locally asymptotically stable for the closed-loop dynamics (3)–(5), (17), (22).*

Proof. The scheme can be represented as the cascade of three hybrid dynamical systems.

The lowermost system corresponds to the dynamics restricted to the set

$$\mathcal{A}_\theta = \{\xi : \theta = \hat{\theta}\},$$

which is clearly forward invariant because the dynamics of $\hat{\theta}$ coincide with that of θ. Using the result of Theorem 1 it is readily seen that the dynamics restricted to $\mathcal{A}_\theta$ is UAS (actually UES) to $\mathcal{A}_e$.

The intermediate system corresponds to the dynamics restricted to the set

$$\mathcal{A}_{\bar{y}} = \{\xi : \bar{y}_r = \bar{b}(0,0) + \frac{3}{\pi}|x_r(0,0)|\}, \tag{24}$$

which is once again forward invariant because one can easily derive from (7) that given any solution to the exosystem (3)–(5), the scalar $\bar{b}(0,0) + \frac{3}{\pi}|x_r(0,0)|$ is the average value of $y_r(t, j^*(t))$ (notice that both $\bar{b}$ and $|x_r|$ remain constant along solutions). Then we may prove that set $\mathcal{A}_\theta$ is uniformly (locally) asymptotically stable for the dynamics restricted to $\mathcal{A}_{\bar{y}}$. To establish this fact we may use the Lyapunov function V_θ in (20) that remains constant along flows (as established in Lemma 3). To analyze the change of V_θ across jumps, first note that in $\mathcal{A}_{\bar{y}}$ we have that $d = y_r - \bar{y}_r$. Then, due to periodicity of timer τ in (22) and due to the results of Lemma 3, we have before each jump in (22b) that $\eta = -|x_r(0,0)|\rho(\tilde{\theta})$. Therefore, across all such jumps, the quantity in (19) satisfies

$$\begin{aligned}(\tilde{\theta}^+)^2 &= \left(\theta - \hat{\theta}^+ + (i^*)^+ \frac{\pi}{3}\right)^2 \\ &\leq \left(\theta - \hat{\theta}^+ + i^* \frac{\pi}{3}\right)^2 \\ &= \left(\tilde{\theta} - \mathrm{sat}_{\frac{\pi}{6}}\left(k_\theta |x_r(0,0)| \rho(\tilde{\theta})\right)\right)^2,\end{aligned}$$

where the inequality follows from the fact that i^* in (18) is a minimizer. Then from uniform boundedness of $|x_r(0,0)|$ and positive definiteness of $\rho(\tilde{\theta})\tilde{\theta}$ in the set $(-\pi/6, \pi/6)$, it is ensured that function V_θ is (locally) strictly decreasing as long as $k_\theta > 0$ is sufficiently small. For all other jumps triggered by the jump sets in (5) and (17), function V_θ remains constant as established in Lemma 3. Since jumps in (22b) are periodic from periodicity of τ, then asymptotic stability of $\mathcal{A}_{\bar{y}}$ follows from persistent jumping and [9, Prop. 3.24].

The uppermost system corresponds to the dynamics starting anywhere in the allowable set of initial conditions, which clearly converge to the attractor in (24) because at each jump triggered by (22b) it holds that $\frac{3\omega}{\pi} y_{rI}$ is the average $\bar{b}(0,0) + \frac{3}{\pi}|x_r(0,0)|$ of y_r, so that the update law at the first equation in (22b) leads to uniform convergence to zero of the Lyapunov function $V_y = (\bar{b} + \frac{3}{\pi}|x_r|)^2$ (once again we apply [9, Prop. 3.24] and persistent jumping to establish this fact). Recall that $\bar{b}$ and $|x_r|$ remain constant along solutions so that V_y remains constant along flows.

Once the three above nested or cascade-like results are established, the uniform (local) asymptotic stability of the innermost attractor given by $\mathcal{A}_e$ in (23) can be established applying iteratively the reasoning in [10, Corollary 19] by intersecting the flow and jump sets with sufficiently large compact sets. □

Remark 7 Notice that one could choose $k_{av} = 1$ in (22b) thereby obtaining finite time convergence of $\bar{y}$ to the (constant) average of y_r. However, smaller choices of k_{av} may be desired to suitably filter possible noise affecting the measurement. Similarly, k_θ should be selected small in such a way to ensure that Theorem 2 applies and that suitable noise rejection is obtained. In general, the tuning of the three parameters k_{av}, k_θ and ℓ should be carried out based on the cascaded structure of the proof. Indeed, to experience a graceful transient performance, it is reasonable to pick gain k_{av} as the most aggressive

one, k_θ in such a way to induce an intermediate speed of convergence, and ℓ as the one that induces the slowest transient. This type of tuning procedure was adopted in the simulation examples of Section 5. ⌟

5 JET experimental measurements

In this Section we apply the scheme in Figure 5, Section 4 to experimental data collected from the JET Tokamak [18]. For simulations that confirm the effectiveness of the method presented in Section 4 in the case of *ideal nonsmooth* signals, we refer the reader to the Simulations Section of [16] while here we focus on the application of the scheme to noisy signals.

The stabilization of the unstable plasma vertical position at JET facilities is achieved by changing the radial magnetic field produced by current flow on dedicated coils. Such a current is regulated by the Vertical Stabilization (VS) system by means of a current amplifier named FRFA (Fast Radial Field Amplifier), that is indeed equipped with the rectifiers discussed in Section 2. The VS system acts on FRFA requesting a desired current $I_{\mathrm{FRFA,des}}$ that is obtained as the sum of two term, the "fast" velocity loop that reacts suddenly to plasma vertical displacements and the "slow" current loop that aims to regulate I_{FRFA} to a given set point value (usually zero). The ripple generated by the FRFA affects the feedback signal Z_{PD}, which is an estimate of the plasma vertical velocity obtained by combining suitable magnetic measurements (from Mirnov coils). We define the signal

$$y_r(t) = \alpha\, I_{\mathrm{FRFA}}(t) + Z_{PD}(t) \tag{25}$$

where $I_{\mathrm{FRFA}}(t)$ is the current flowing within the poloidal coil and the scaling factor α is equal to $4 \cdot 10^4$ m/s/A. All these quantities are depicted in Figure 7 where the effect of the ripple is evident on y_r.

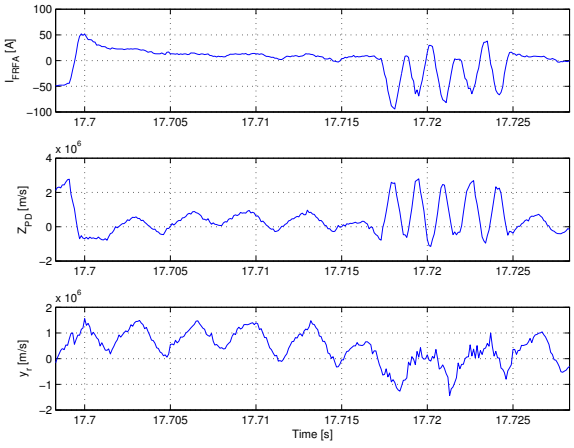

Figure 7. Experiment data from JET Tokamak: current I_{FRFA}, estimated vertical velocity Z_{PD} of plasma and measured signal y_r.

To obtain a ripple-free signal, we apply the scheme in Figure 5 where we discard the "Signal with ripple disturbance" block and we inject directly into the "Ripple observer" block the signal y_r in (25). As a matter of fact we have no longer a constant signal over which the ripple disturbance is superposed, but a signal that varies slowly with respect to the frequency of the ripple. Nevertheless, since we are taking compact sets and sufficiently regular data in the hybrid system formulation, we can rely on the robustness results of [9, Ch. 7], as we stated earlier in this paper.

The experimental data we consider are only a 20 second portion of the out of the 80 seconds available in pulse ♯78000 because the remaining 60 s do not correspond to relevant experimental data. For these 20 seconds we zoom towards the end of the simulation (at about 17.70 s), as in Figure 7. Although we test our hybrid observer on offline experimental data, we would like to point out that it could be used for estimating the ripple *on-line*, which would allow to improve the quality of the measured signal and thus the performance of the vertical stabilization loop.

In [16] we noted that we should implement slightly inflated versions of flow and jump sets $\mathcal{C}$ and $\mathcal{D}$ in (5) to force the simulated maximal hybrid solutions to be also complete [9, Ch. 2.2 and 2.3]. Otherwise we may simulate maximal solutions that terminate prematurely (are not complete) because the numerical perturbations force them to fall outside $\mathcal{C} \cup \mathcal{D}$. In the current case of JET measurements we no longer have a ripple generator, and for the flow/jump sets in (17) and in (22) we only inflated the jump set $\{\xi\colon \tau = \frac{\pi}{3\omega}\}$ as $\{\xi\colon \frac{\pi}{3\omega} \leq \tau \leq 1.005\frac{\pi}{3\omega}\}$.

We choose the values $\ell = 7.5$, $k_{av} = 0.9$, $k_\theta = 1$ as parameters of our hybrid observer described in (17) and (22) and we initialize it with $\bar{y}_r(0) = -0.5 \cdot 10^6$, $\bar{y}_{rI} = 0$, $\eta(0) = 0, \tau(0) = 0, \hat{\theta} = 0, x_f(0) = \left[\begin{smallmatrix}0\\0\end{smallmatrix}\right], \hat{x}_r(0) = \left[\begin{smallmatrix}9.6\cdot 10^6\\0\end{smallmatrix}\right]$.

Analogously with the results in Section 4, we use as estimated signal $\hat{\sigma} = y_r - \left(\hat{x}_{r1} - \frac{3}{\pi}|\hat{x}_r|\right)$. At the bottom of Figure 8 we have both y_r and $\hat{\sigma}$ on the full time scale. In the above part, we have a zoom at the beginning of the time history on the left, and at the end of the time history on the right (same zoom as in Figure 7). The red vertical lines correspond to the instants when $\hat{\theta}$ jumps and it is shown clearly that at the beginning they are not in phase with the original signal y_r while at the end they are, so that the hybrid observer effectively removes from y_r the ripple disturbance d depicted in the middle part of Figure 8.

6 Conclusions

We proposed a hybrid system to model the ripple phenomenon that arises in different contests such as power

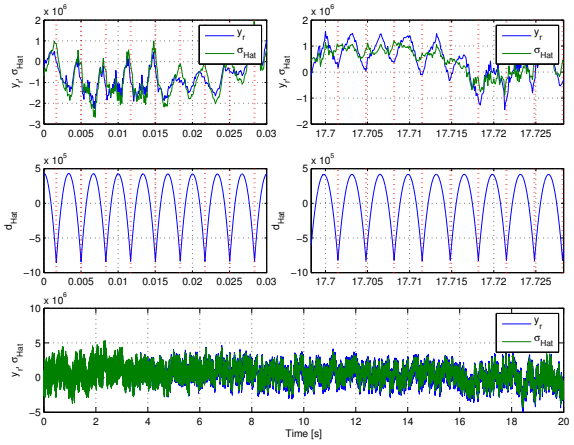

Figure 8. Original signal y_r, signal $\hat{\sigma}$ deprived of the ripple and ripple $\hat{d}$ estimated by the hybrid observer in different time scales.

electronics. We discussed the effectiveness of the proposed hybrid model characterizing its (hybrid) solutions, flow/jump dynamics and flow/jump sets. We proposed two hybrid schemes able to asymptotically estimate the state of the hybrid model that generates the ripple waveform both when the switching instants are known and unknown. The proposed methodology was applied to reconstruct the ripple disturbance affecting experimental data of the vertical stabilization system at JET facilities.

References

[1] A. Pironti and M. Walker. Fusion, tokamaks, and plasma control: an introduction and tutorial. *Control Systems Magazine, IEEE*, 25(5):30–43, 2005.

[2] Bruce A Francis and W Murray Wonham. The internal model principle of control theory. *Automatica*, 12(5):457–465, 1976.

[3] A. Isidori. *Nonlinear Control Systems*. Springer, third edition, 1995.

[4] Lorenzo Marconi and Andrew R Teel. A note about hybrid linear regulation. In *IEEE Conference on Decision and Control*, pages 1540–1545. IEEE, 2010.

[5] Nicholas Cox, Lorenzo Marconi, and Andrew Teel. High-gain observers and linear output regulation for hybrid exosystems. *International Journal of Robust and Nonlinear Control*, 2013.

[6] Lorenzo Marconi and Andrew R Teel. Internal model principle for linear systems with periodic state jumps. *IEEE Transactions on Automatic Control*, 58(11):2788–2802, 2013.

[7] Daniele Carnevale, Sergio Galeani, and Laura Menini. Output regulation for a class of linear hybrid systems. parts 1 & 2. In *IEEE Conference on Decision and Control*. IEEE, 2012.

[8] D. Carnevale, S. Galeani, and M. Sassano. Necessary and sufficient conditions for output regulation in a class of hybrid linear systems. In *Decision and Control (CDC), 2013 IEEE 52nd Annual Conference on*, pages 2659–2664, Dec 2013.

[9] R. Goebel, R.G. Sanfelice, and A.R. Teel. *Hybrid Dynamical Systems: modeling, stability, and robustness*. Princeton University Press, 2012.

[10] R. Goebel, R. Sanfelice, and A.R. Teel. Hybrid dynamical systems. *IEEE Control Systems Magazine*, 29(2):28–93, April 2009.

[11] Nicholas Cox, Lorenzo Marconi, and Andrew R Teel. Hybrid output regulation with unmeasured clock. In *Joint IEEE Conference on Decision and Control and Europen Control Conference*, pages 7410–7415, 2011.

[12] F. Forni, A.R. Teel, and L. Zaccarian. Follow the bouncing ball: global results on tracking and state estimation with impacts. *IEEE Transactions on Automatic Control*, 58(6):1470–1485, 2013.

[13] A.R. Teel, F. Forni, and L. Zaccarian. Lyapunov-based sufficient conditions for exponential stability in hybrid systems. *IEEE Transactions on Automatic Control*, 58(6):1591–1596, 2013.

[14] F. Forni, A.R. Teel, and L. Zaccarian. Reference mirroring for control with impacts. In J. Daafouz, S. Tarbouriech, and M. Sigalotti, editors, *Hybrid Systems with Constraints*, pages 211–249. Wiley, 2013.

[15] Lorenzo Marconi and Laurent Praly. Uniform practical nonlinear output regulation. *IEEE Transactions on Automatic Control*, 53(5):1184–1202, 2008.

[16] A. Bisoffi, M. Da Lio, and L. Zaccarian. A hybrid ripple model and two hybrid observers for its estimation. In *IEEE Conference on Decision and Control*, Los Angeles (CA), USA, December 2014.

[17] Christopher G Mayhew, Ricardo G Sanfelice, and Andrew R Teel. Quaternion-based hybrid control for robust global attitude tracking. *IEEE Transactions on Automatic Control*, 56(11):2555–2566, 2011.

[18] F Sartori, A Barbalace, AJN Batista, T Bellizio, P Card, G De Tommasi, P Mc Cullen, A Neto, F Piccolo, R Vitelli, et al. The pcu jet plasma vertical stabilization control system. *Fusion Engineering and Design*, 85(3):438–442, 2010.